Validation of a time domain impedance formulation for the case of a 2D rectangular lined duct with a non-uniform mean-flow with a finite boundary layer thickness

A. Ammirati [1], **H. Denayer**[1], **W. De Roeck**[1], **W. Desmet**[1]
[1] KU Leuven, Department of Mechanical Engineering,
Celestijnenlaan 300 B, B-3001, Heverlee, Belgium
e-mail: **antonio.ammirati@mech.kuleuven.be**

Abstract

A validation and improvement of a recently developed time domain impedance formulation based on recursive convolution has been carried out. This formulation has been implemented using an in-house time-domain Runge-Kutta Discontinous Galerkin (RKDG) Linearized Euler Equations (LEE) solver.
At first, a validation has been carried out on a $2D$ lined rectangular duct both without flow and with uniform mean flow. The RKDG results have been compared with the analytical reference solutions for the problem under consideration. In a second stage the case of the $2D$ rectangular lined duct with a non-uniform mean flow is validated to include the effect of a finite boundary layer thickness on the acoustic damping properties.

1 Introduction

Lining materials play an important role in many aeroacoustic applications to control the emitted noise level. During the design process, numerical models are of crucial importance to evaluate the effect of different lining material and to carry out sensitivity analysis of different material and geometrical parameters. In a numerical setup, a lining material is typically characterized by the impedance or its inverse, the admittance. The impedance is a material property, valid in the linear regime, defined in frequency domain as the ratio of the complex acoustic pressure and normal velocity at a certain point of the lined surface

$$P(\omega, x_b) = Z(\omega)V(\omega, x_b); \quad V(\omega, x_b) = A(\omega)P(\omega, x_b) \tag{1}$$

The impedance is typically obtained experimentally by identifying the forced response of the material under a single frequency excitation. It is therefore typically available for a limited set of discrete frequencies. The aeroacoustic phenomena are governed by the Linearized Euler Equations (LEE) and Linearized Navier-Stokes Equations (LNSE), obtained from a linearization of the Navier-Stokes equations under the assumption that the acoustic variables are of some order of magnitude smaller than the mean flow variables. These equations are expressed in time-domain and constitute the basis of computational areo-acoustics (CAA). Time-domain computational methods have a clear advantage over frequency-domain for transient wave simulations, large scale problems, non-linear investigations and broadband problems. In time-domain the relations

(1) correspond to a convolution product:

$$\begin{aligned} p(t,x_b) &= z(t) * v(t,x_b) = \int_{-\infty}^{\infty} z(\tau)v(t-\tau,x_b)d\tau \\ v(t,x_b) &= a(t) * p(t,x_b) = \int_{-\infty}^{\infty} a(\tau)p(t-\tau,x_b)d\tau \end{aligned} \tag{2}$$

where

$$\begin{aligned} z(t) &= \int_{-\infty}^{\infty} Z(\omega)e^{j\omega t}d\omega \\ a(t) &= \int_{-\infty}^{\infty} A(\omega)e^{j\omega t}d\omega \end{aligned} \tag{3}$$

Due to the presence of the convolution, it is more difficult to model the impedance in time domain than in frequency domain. Computing a full convolution, requires the storage of the full time history of the data, which is costly in terms of memory and CPU time. Reymen et al. [1] described a generic time-domain impedance formulation based on the recursive convolution method. Under some assumptions, the convolution can be easily computed by means of complex-valued accumulators.

The aim of this work is to improve and to validate this formulation. In particular, the capability of this boundary condition to take into account typical flow-acoustic phenomena occurring in flow duct systems, such as the presence of a mean-flow with a finite boundary layer, is analyzed. The case of a $2D$ rectangular duct with a single lined wall is studied. To check the stability of the formulation, at first the cases of a duct of different length with no-flow and with uniform mean-flow up to Mach number 0.1 are studied. At a second stage a non uniform mean-flow with a parabolic profile in the boundary layer has been used. For all the cases under investigation, a single frequency model for the admittance is used (appendix A).

This formulation for the time-domain admittance boundary condition, improved here to account for non uniform substages within uniform time steps, has been implemented in an in-house Runge Kutta Discontinuous Galerkin (RKDG) solver for Linearized Euler Equations (LEE). The RKDG solver has the capability to model both $2D$ and $3D$ geometries involving a non-uniform mean flow. The solution is approximated by elements of arbitrary order p, where the solution in each element is represented by its components in a polynomial basis of order p. In the case of a non-uniform mean flow, obtained from CFD simulations or from analytical solutions, the mean-flow is represented by its components in the same polynomial basis. A least square approach is used to fit the approximate components to the ideal solution [2]. For the temporal discretization, an 8-stage Runge-Kutta fourth order scheme, optimized for maximum stable time step, is used (RK84C)[3].

2 Time-Domain impedance formulation

After discretization of the time axis in equal time steps Δt the convolution product (eq. (2)) after n time steps can be written as:

$$p(n\Delta t) = \int_0^{n\Delta t} z(\tau)v(n\Delta t-\tau)d\tau; \qquad v(n\Delta t) = \int_0^{n\Delta t} a(\tau)p(n\Delta t-\tau)d\tau. \tag{4}$$

To compute this convolution the time domain impedance $z(\tau)$ or admittance $a(\tau)$ need to be known (3). The impedance, which characterizes the lining material, is most often known only for a discrete number of

frequencies. However, the inverse Fourier transform of (3) requires the knowledge of the impedance over the full frequency axis. It is, therefore necessary to introduce a frequency domain impedance model which has to comply with the 3 necessary conditions (causality, reality and passivity), indicated by Rienstra [4], for the model to be physically feasible. Such a model can be obtained by approximating the impedance using a finite number of first and second order systems.

$$A(\omega) = \sum_{K=1}^{S} \frac{B_k}{j\omega + \lambda_k} + \sum_{l=1}^{T} \frac{C_l(j\omega) + D_l}{(j\omega + \alpha_l)^2 + \beta_l^2} \qquad \lambda_k \geq 0, \;\; \alpha_l \geq 0 \tag{5}$$

Where B_k, C_l and D_l are the residues of the first and second order systems and λ_k and $\alpha \pm j\beta$ are the poles of the first and second order system. This optimal fit can be obtained in different ways, such as the single frequency and the ad-hoc broadband model [5]. Using equations (3) and (5) a time-domain impedance formulation is straightforward to obtain.

$$a(t) = \sum_{K=1}^{S} z_k(t) + \sum_{l=1}^{T} z_l(t), \qquad \lambda_k \geq 0, \;\; \alpha_l \geq 0 \tag{6}$$

$$= \sum_{K=1}^{S} B_k e^{-\lambda_k t} H(t) + \sum_{l=1}^{T} e^{-\alpha_l t} \left(C_l \cos \beta_l t + \frac{D_l - \alpha_l C_l}{\beta_l} \sin \beta_l t \right) H(t), \qquad \lambda_k \geq 0, \;\; \alpha_l \geq 0 \tag{7}$$

After some math equation (7) can be simplified introducing constant K_{1l} and K_{2l}.

$$= \sum_{K=1}^{S} B_k e^{-\lambda_k t} H(t) + \sum_{l=1}^{T} \left(K_{1l} \Re \left\{ e^{(-\alpha_l + j\beta_l)t} \right\} + K_{2l} \Im \left\{ e^{(-\alpha_l + j\beta_l)t} \right\} \right) H(t), \qquad \lambda_k \geq 0, \;\; \alpha_l \geq 0 \tag{8}$$

Where $H(t)$ is the Heaviside function. Using this expression, and assuming the normal pressure (velocity) to be piecewise constant or linear within a time step, the recursive convolution can be easily computed by means of complex-valued accumulators.

2.1 Recursive convolution

Equation (4) assumes the time steps Δt to be of equal length. The integration scheme used in the RKDG solver is an 8-stage Runge-Kutta fourth order scheme and so an extension to account for non uniform sub-stages within the time steps is presented in this section. It is assumed that the time-axis is discretized using a multi-stage explicit time-integration scheme, with a constant time step Δt, subdivided in a number of stages whose length is not necessarily equal (figure 1). This means that the convolution integral has to be evaluated at discrete time values $t^{n,s} = n\Delta t + \delta t^s$, with δt^s the length of the current substage s. With this assumption, the convolution integral (2) can be written in a discrete form:

$$\begin{aligned} v(t^{n,s}) = a(t^{n,s}) * p(t^{n,s}) &= \int_0^{t^{n,s}} a(\tau) p(t^{n,s} - \tau)\, d\tau \\ &= \int_0^{\delta t^s} a(\tau) p(t^{n,s} - \tau)\, d\tau + \int_{\delta t^s}^{t^{n,s}} a(\tau) p(t^{n,s} - \tau)\, d\tau \\ &= \int_0^{\delta t^s} a(\tau) p(n\Delta t + \delta t^s - \tau)\, d\tau + \sum_{m=0}^{n-1} \int_{m\Delta t}^{(m+1)\Delta t} a(\tau + \delta t^s) p(n\Delta t - \tau)\, d\tau \end{aligned} \tag{9}$$

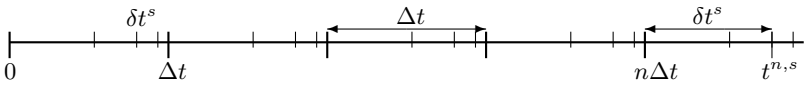

Figure 1: Discretized time axis

The convolution integral is now split in an integral over the current time step (up to the current substage) and a sum of integrals over each of the previous time steps.

To compute these integrals, an assumption is needed regarding the behavior of the pressure in between two time steps. By analogy to the time-domain impedance model by Reymen et al. [1] a piecewise linear behavior is assumed within each sub time step:

$$p(t) = p^m + \frac{p^{m+1} - p^m}{\Delta t}\,(t - t^m) \qquad\qquad t \in [m\Delta t, (m+1)\Delta t] \tag{10}$$

The convolution requires the pressure to be written as a function of the reverse time, shifted with $n\Delta t$:

$$p(n\Delta t - \tau) = p^{n-m} + \frac{p^{n-m-1} - p^{n-m}}{\Delta t}\,(\tau - t^m) \qquad\qquad \tau \in [m\Delta t, (m+1)\Delta t] \tag{11}$$

Introducing this assumption and the model (8) for the admittance in the second part of equation (9) gives after some algebraic manipulations:

$$\begin{aligned}\sum_{m=0}^{n-1} \int_{m\Delta t}^{(m+1)\Delta t} a(\tau + \delta t^s) p(n\Delta t - \tau)\, d\tau &= \sum_{k=0}^{S} B_k\, e^{-\lambda_k \delta t^s} \sum_{m=0}^{n-1} \left(p^{n-m}\chi_k^m + \left(p^{n-m-1} - p^{n-m}\right)\xi_k^m\right) \\ &+ \sum_{l=0}^{T} K_{1l}\, \Re\left\{ e^{(-\alpha_l + j\beta_l)\delta t^s} \sum_{m=0}^{n-1} \left(p^{n-m}\hat{\chi}_l^m + \left(p^{n-m-1} - p^{n-m}\right)\hat{\xi}_l^m\right)\right\} \\ &+ \sum_{l=0}^{T} K_{2l}\, \Im\left\{ e^{(-\alpha_l + j\beta_l)\delta t^s} \sum_{m=0}^{n-1} \left(p^{n-m}\hat{\chi}_l^m + \left(p^{n-m-1} - p^{n-m}\right)\hat{\xi}_l^m\right)\right\},\end{aligned} \tag{12}$$

where

$$\chi_k^m = \int_{m\Delta t}^{(m+1)\Delta t} e^{-\lambda_k \tau}\, d\tau \qquad\qquad \xi_k^m = \frac{1}{\Delta t} \int_{m\Delta t}^{(m+1)\Delta t} e^{-\lambda_k \tau}\,(\tau - m\Delta t)\, d\tau$$

$$\hat{\chi}_l^m = \int_{m\Delta t}^{(m+1)\Delta t} e^{(-\alpha_l + j\beta_l)\tau}\, d\tau \qquad\qquad \hat{\xi}_l^m = \frac{1}{\Delta t} \int_{m\Delta t}^{(m+1)\Delta t} e^{(-\alpha_l + j\beta_l)\tau}\,(\tau - m\Delta t)\, d\tau.$$

For every time step, these variables can be computed recursively from their value at the previous time step (shown in appendix B):

$$\begin{aligned}\chi_k^{m+1} &= e^{-\lambda_k \Delta t}\,\chi_k^m & \qquad \hat{\chi}_l^{m+1} &= e^{(-\alpha_l + j\beta_l)\Delta t}\,\hat{\chi}_l^m \\ \chi_k^{m+1} &= e^{-\lambda_k \Delta t}\,\chi_k^m & \qquad \hat{\xi}_l^{m+1} &= e^{(-\alpha_l + j\beta_l)\Delta t}\,\hat{\xi}_l^m\end{aligned} \tag{13}$$

By defining the accumulators ψ_k^n and $\hat{\psi}_l^n$:

$$\psi_k^n = \sum_{m=0}^{n-1} \left(p^{n-m}\chi_k^m + \left(p^{n-m-1} - p^{n-m}\right)\xi_k^m\right) \tag{14}$$

$$\hat{\psi}_l^n = \sum_{m=0}^{n-1} \left(p^{n-m}\hat{\chi}_l^m + \left(p^{n-m-1} - p^{n-m}\right)\hat{\xi}_l^m\right), \tag{15}$$

The second part of the integral (9) can be computed as:

$$\sum_{m=0}^{n-1} \int_{m\Delta t}^{(m+1)\Delta t} a(\tau + \delta t^s) p(n\Delta t - \tau)\, d\tau$$
$$= \sum_{k=0}^{S} B_k\, e^{-\lambda_k \delta t^s}\, \psi_k^n + \sum_{l=0}^{T} \left(K_{1l}\, \Re\left\{ e^{(-\alpha_l + j\beta_l)\delta t^s}\, \hat{\psi}_l^n \right\} + K_{2l}\, \Im\left\{ e^{(-\alpha_l + j\beta_l)\delta t^s}\, \hat{\psi}_l^n \right\} \right), \quad (16)$$

where the properties (13) are applied to compute the value of the accumulators in a recursive way (shown in appendix C):

$$\psi_k^n = p^n \chi_k^0 + \left(p^{n-1} - p^n\right) \xi_k^0 + e^{-\lambda_k \Delta t}\, \psi_k^{n-1} \quad \hat{\psi}_l^n = p^n \hat{\chi}_l^0 + \left(p^{n-1} - p^n\right) \hat{\xi}_l^0 + e^{(-\alpha_l + j\beta_l)\Delta t}\, \hat{\psi}_l^{n-1} \quad (17)$$

This corresponds to the recursive convolution of Reymen et al. [1]. For the computation of the first part of the integral in equation (9), assumption (11) would result in an implicit time-integration scheme. To keep the scheme explicit, the slope of the linear behavior of the pressure within the current time step is estimated using the pressure at the current stage:

$$p(t) = p^n + \frac{p^{n,s} - p^n}{t^{n,s} - t^n} \left(t - t^n\right) \qquad t \in [n\Delta t, n\Delta t + \delta t^s = t^{n,s}] \quad (18)$$

As a function of the reverse time, shifted by $t^{n,s}$:

$$p(t^{n,s} - \tau) = p^{n,s} + \frac{p^n - p^{n,s}}{\delta t^s}\, \tau \qquad \tau \in [0, \delta t^s] \quad (19)$$

Introducing this assumption, together with the model (8) for the admittance into the first part of equation (9):

$$\int_0^{\delta t^s} a(\tau) p(n\Delta t + \delta t^s - \tau)\, d\tau = \sum_{k=1}^{S} B_k \left(p^{n,s} \int_0^{\delta t^s} e^{-\lambda_k \tau}\, d\tau + \left(p^n - p^{n,s}\right) \frac{1}{\delta t^s} \int_0^{\delta t^s} e^{-\lambda_k \tau}\, \tau\, d\tau \right)$$
$$+ \sum_{l=1}^{T} K_{1l}\, \Re\left\{ p^{n,s} \int_0^{\delta t^s} e^{(-\alpha_l + j\beta_l)\tau}\, d\tau + \left(p^n - p^{n,s}\right) \frac{1}{\delta t^s} \int_0^{\delta t^s} e^{(-\alpha_l + j\beta_l)\tau}\, \tau\, d\tau \right\}$$
$$+ \sum_{l=1}^{T} K_{2l}\, \Im\left\{ p^{n,s} \int_0^{\delta t^s} e^{(-\alpha_l + j\beta_l)\tau}\, d\tau + \left(p^n - p^{n,s}\right) \frac{1}{\delta t^s} \int_0^{\delta t^s} e^{(-\alpha_l + j\beta_l)\tau}\, \tau\, d\tau \right\}, \quad (20)$$

The integrals in this equation are recurring in every time step. It is hence sufficient to compute these constants only once for all stage lengths δt^s:

$$I_k^s = \frac{1 - e^{-\lambda_k \delta t^s}}{\lambda_k} \qquad J_k^s = \frac{e^{-\lambda_k \delta t^s} \left(-\lambda_k \delta t^s - 1\right) + 1}{\lambda_k^2 \delta t^s} \quad (21)$$

$$\hat{I}_l^s = \frac{1 - e^{(-\alpha_l + j\beta_l)\delta t^s}}{\alpha_l - j\beta_l} \qquad \hat{J}_l^s = \frac{e^{(-\alpha_l + j\beta_l)\delta t^s} \left((-\alpha_l + j\beta_l)\delta t^s - 1\right) + 1}{(-\alpha_l + j\beta_l)^2 \delta t^s} \quad (22)$$

Recombining equations (16) and (20), The convolution integral can now be computed as the sum of a recursively computed part, accounting for the previous time steps, and a term depending on the current time

step:

$$v(t^{n,s}) = a(n\Delta t + \delta t^s) * p(n\Delta t + \delta t^s) = \sum_{k=1}^{S} B_k \left(e^{-\lambda_k \delta t^s} \psi_k^n + p^{n,s} I_k^s + (p^n - p^{n,s}) J_k^s \right) + \sum_{l=1}^{T} K_{1l} \Re \left\{ e^{(-\alpha_l + j\beta_l)\delta t^s} \hat{\psi}_l^n + p^{n,s} \hat{I}_l^s + (p^n - p^{n,s}) \hat{J}_l^s \right\} + \sum_{l=1}^{T} K_{2l} \Im \left\{ e^{(-\alpha_l + j\beta_l)\delta t^s} \hat{\psi}_l^n + p^{n,s} \hat{I}_l^s + (p^n - p^{n,s}) \hat{J}_l^s \right\} \quad (23)$$

When computing the integral at the beginning of a time step ($\delta t^s = 0$), only the terms depending on the accumulator functions remain. These accumulators are updated using the information from the previous time step. In the other substages, the value of the accumulators is not changed, only additional terms, depending on the current stage length, are taken into account. The derivation for an impedance boundary condition is similar and can be obtained by switching the role of p and v.

The formulation for the admittance boundary condition refers to a general frequency domain admittance model. In the simulations a single frequency impedance model is used (shown in appendix A).

3 Validation study cases

In order to validate the improved time domain impedance boundary condition, the case of a $2D$ rectangular duct with a single lined wall, both without flow and with uniform mean flow, is analyzed. At a second stage, the case of a non uniform mean flow is investigated to account for the presence of a finite boundary layer. The RKDG results have been compared with an analytic reference solution [6, 7, 8] based on the assumption that only plane wave in the downstream direction can propagate inside the duct.

3.1 No flow and uniform mean-flow cases

3.1.1 Problem description

To define the operational interval of the implemented code, the case of a $2D$ rectangular duct both without and with uniform mean-flow up to a Mach number $M = 0.1$ have been analyzed. The configuration under investigation has a height equal to $b = 0,05m$ and a varying length L corresponding to $0.4m$, $0.6m$, $0.8m$ and $1m$. The duct is lined at the bottom wall. Impedance boundary conditions at 6 different frequencies ($500Hz$, $1000Hz$, $1500Hz$, $2000Hz$, $2500Hz$, $3000Hz$) are analyzed with a frequency independent non dimensional impedance of $Z = 1,06 - 1.29j$. At the other walls a rigid wall boundary condition is imposed, in combination with a characteristic non reflecting boundary condition at the downstream end. The impedance boundary condition is tested for different types of excitations: a characteristic plane mode boundary condition at different frequencies (the same used for the impedance model) and a pulse excitation. Because of the time domain approach a pulse excitation is faster and lighter to compute, saving CPU time than a single frequency excitation. Moreover, a pulse excitation is better for the acoustic characterization of broadband phenomena. Hence, these simulations represent an ideal starting point for future validations of the broadband impedance model. The results of the simulations have been obtained for different monitor points (MP) along the axis of the duct. The MPs are separated by a distance of $0.01m$ from each other starting from the a point on the horizontal axis $0.01m$ from the inlet. As a result there are $40MPs$ for the $0.4m$ duct, $60MPs$ for the $0.6m$ duct,$80MPs$ for the $0.8m$ duct and $100MPs$ for the $1m$ duct. A sketch of the configuration is shown in figure 2. For the simulations with the RKDG solver,a unstructured mesh consisting of triangular elements of order $p = 6$ is used. There are 70 elements for the $0.4m$ duct, 102 elements for the $0.6m$ duct, 134 elements for the $0.8m$ duct, 166 elements for the $1m$ duct.

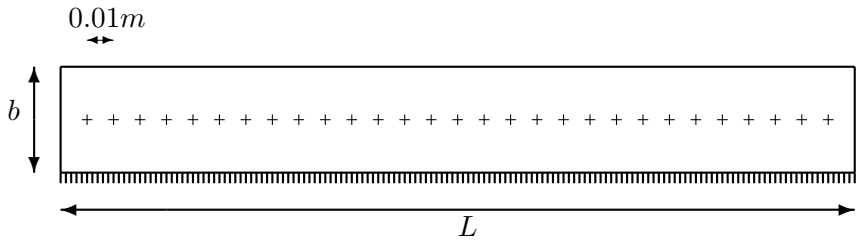

Figure 2: Duct configuration

3.1.2 Discussion of the results

Figure 3 shows the acoustic pressure amplitude, non-dimensionalized by $\rho_\infty c_\infty^2$ (with ρ_∞ and c_∞ , respectively, the reference mean flow density and speed of sound, along the centerline of the duct), for the case without flow for all the frequencies investigated and for all the different lengths of the duct. All the curves show an exponential decay in the downstream direction, as expected, but for some of them some fluctuations are present. This behavior is only present for the shorter lengths and for higher wave lengths λ of the excitation. In fact, these oscillations disappear as soon as the ratio $\lambda/L < 0.4$ (see tab.1). This phenomenon is most probably due to some resonances caused by the interaction of the impedance boundary layer and the non reflecting boundary condition downstream.

λ/L	$\lambda = 0.68m$	$\lambda = 0.34m$	$\lambda = 0.229m$	$\lambda = 0.172m$	$\lambda = 0.137m$	$\lambda = 0.114m$
$L = 0.4$	1.72	0.86	0.57	0.43	0.34	0.28
$L = 0.6$	1.14	0.57	0.38	0.28	0.22	0.19
$L = 0.8$	0.86	0.43	0.28	0.21	0.17	0.14
$L = 1$	0.68	0.34	0.22	0.17	0.13	0.11

Table 1: λ/L ratio for the no flow cases

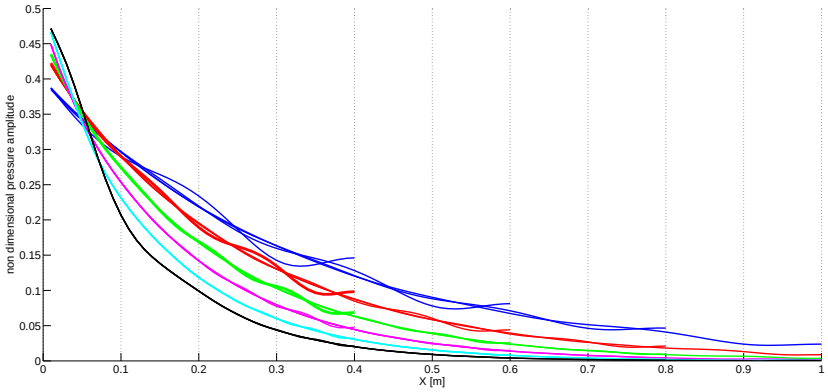

Figure 3: Non-dimensional acoustic pressure amplitude along the centerline of the duct, using plane mode excitation, without mean flow (- $500Hz$, - $1000Hz$,- $1500Hz$, - $2000Hz$, - $2500Hz$, - $3000Hz$)

The same behavior is obtained for the simulation with uniform mean flow at $M = 0.1$, as shown in figure 4.

The results obtained from DG simulations are compared with an analytic reference solution [6] for which only upstream plane wave propagation is occurring in the duct. The pressure in both the simulations and the analytic solutions is normalized by the complex pressure on the first MP ($x = 0.01m$) both for amplitude

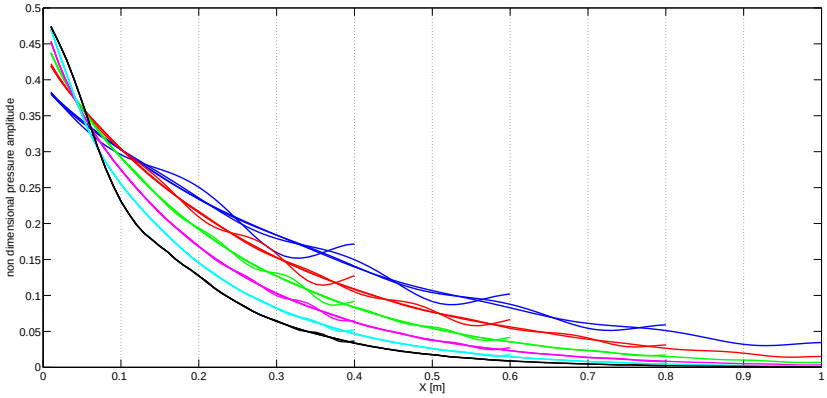

Figure 4: Non-dimensional acoustic pressure amplitude along the centerline of the duct, using plane mode excitation, for uniform mean flow (- $500Hz$, - $1000Hz$,- $1500Hz$, - $2000Hz$, - $2500Hz$, - $3000Hz$)

and phase. Based on this assumption, once the wall impedance Z_w is known, it is possible to retrieve the axial and transvers wave numbers k_x and k_y and the resulting normalized pressure amplitude along the length of the duct. Figures 5 and 6, referring to the case of $L = 0.8m$, show for different conditions that the DG results are in excellent agreement with the reference solution for both the case of a plane mode excitation and the pulse excitation. The underprediction of the numerical results should be avoided by reducing the size of the element in the mesh.

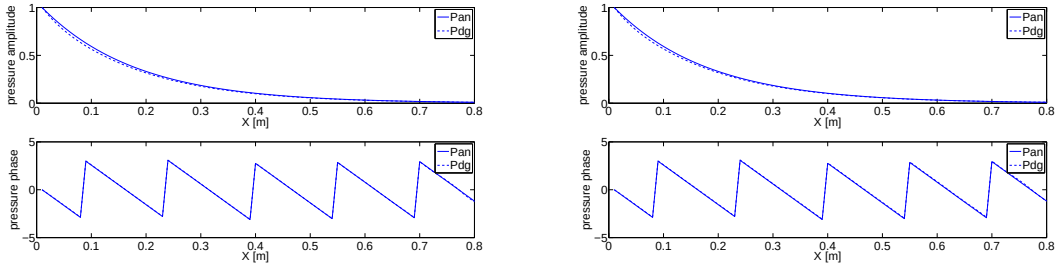

(a) Plane mode excitation at $2000Hz$ (b) Pulse excitation, result at $2000Hz$

Figure 5: Comparison of the DG result with the analytical reference solution for a no flow case (– analytical solution, - - DG solution)

In order to further verify the implementation of the impedance boundary condition, the impedance wall value Z_{wr}, is computed from the DG results and compared with the imposed value. Based on the same assumptions as above, k_x has been calculated from the DG data and used to obtain k_y and Z_{wr}. As can been noticed on figure 7 and 8, the relative error between the retrieved value Z_{wr} and Z_w over the frequencies for different duct lengths is always smaller than 6% as long, as $\lambda/L > 0.4$ for both the case of plane mode excitation and for pulse excitation.

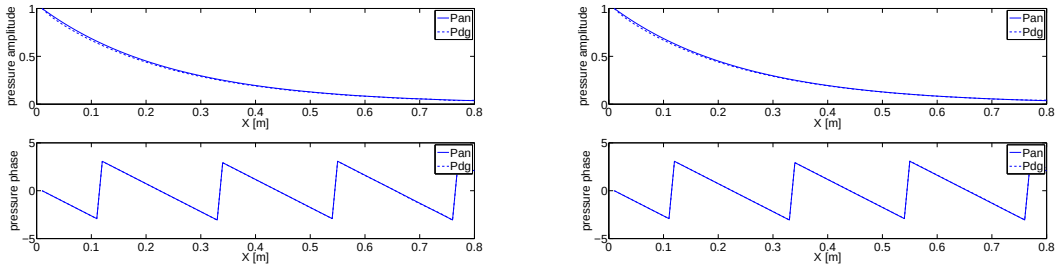

(a) Plane mode excitation at $1500Hz$ (b) Pulse excitation, result at $1500Hz$

Figure 6: Comparison of the DG result with the analytical reference solution for a uniform mean flow case (– analytical solution, - - DG solution)

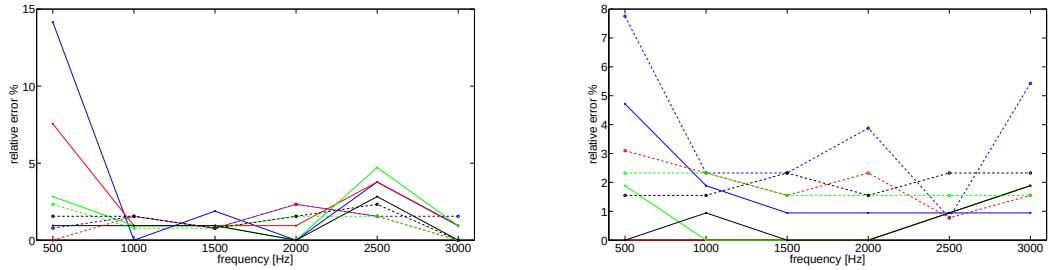

(a) Plane mode excitation (b) Pulse excitation

Figure 7: Relative error between Z_{wr} and Z_w as a function of frequency for simulations without mean flow (– $L = 0.4m$ real part, – $L = 0.6m$ real part, – $L = 0.8m$ real part, – $L = 1m$ real part, - - $L = 0.4m$ imaginary part, - - $L = 0.6m$ imaginary part, - - $L = 0.8m$ imaginary part, - - $L = 1m$ imaginary part)

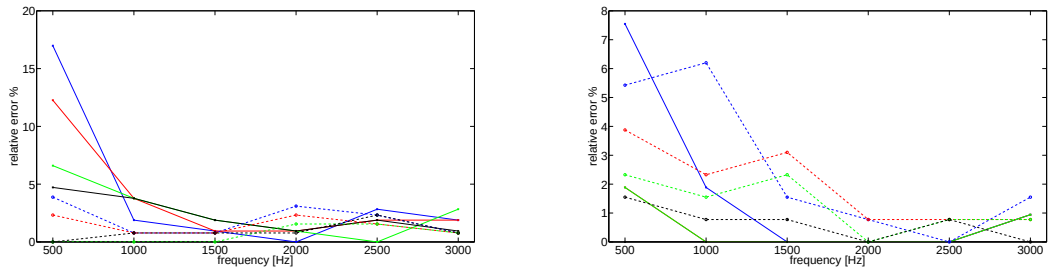

(a) Plane mode excitation (b) Pulse excitation

Figure 8: Relative error between Z_{wr} and Z_w as a function of frequency for simulations with uniform mean flow (– $L = 0.4m$ real part, – $L = 0.6m$ real part, – $L = 0.8m$ real part, – $L = 1m$ real part, - - $L = 0.4m$ imaginary part, - - $L = 0.6m$ imaginary part, - - $L = 0.8m$ imaginary part, - - $L = 1m$ imaginary part)

3.2 Non uniform mean-flow

3.2.1 Problem Description

In order to investigate if the implemented time-domain impedance boundary condition is capable of accounting for the presence of a finite boundary layer in the mean-flow the simulations described above are also carried out for a non uniform mean flow. As for the previous cases, a $2D$ rectangular duct fully lined on the bottom wall is analyzed. The duct has a height of $0,05m$ and a length equal to $0.6m$. A single frequency impedance boundary condition at $2000Hz$ and $2500Hz$ is used with the same non-dimensional value as for the uniform mean flow cases. The top wall is a rigid wall with a slip boundary condition. At the outlet (right side) a characteristic non reflecting boundary condition is imposed. The impedance boundary condition is tested for different type of excitation: first, a characteristic plane mode boundary condition at the same frequency as the ones studied for the impedance is imposed at the inlet (upstream end), afterward a pulse excitation has been used. The mean flow profile is parabolic in the boundary layer, with a Mach number for the mean flow velocity rising from $M = 0$ at the walls up to $M = M_0$ at the extremity of the parabolic boundary layer. A uniform mean flow with a Mach number $M = M_0$ is imposed outside the boundary layer. Different values of M_0 have been taken into account (0.01, 0.04, 0.08, 0.1).The boundary layer thickness is chosen to be $1/10$ of the height of the duct. A sketch of the mean flow profile inside the duct is shown in figure 9. For the simulations triangular element of order $p = 6$ are used. The mesh is composed of 5264 elements with a finer mesh in the boundary layer.

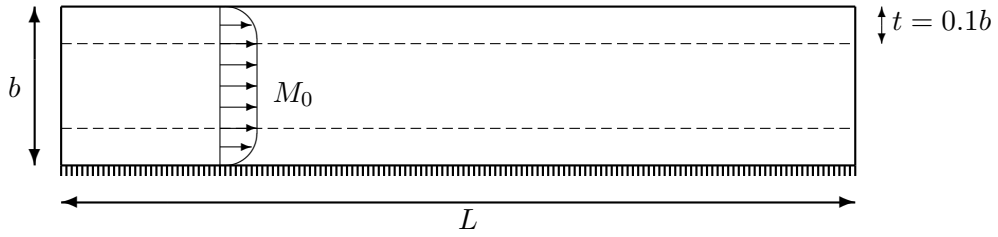

Figure 9: Mean-flow profile

3.2.2 Discussion of the results

The results obtained from the DG simulations are validated by comparing the wall impedance, retrieved from the DG data (Z_{wr}), with the one imposed as boundary condition (Z_w). To determine Z_{wr} from the DG results the same approach used by Enghardt and Fischer [7] is adopted. Starting from the value of the acoustic pressure on the rigid wall and assuming that only downstream wave propagation is occurring inside the duct, k_x is calculated and used to integrate the Pridmore-Brown equation [8] to get the acoustic pressure and normal velocity on the lined wall and to estimate the impedance Z_{wr}. In figure 10, the relative error between the retrieved value Z_{wr} and Z_w as a function of frequency for different values of M_0 and for both plane wave and pulse excitation are shown. The relative error rate is very small (i.e. smaller than 3.5%).

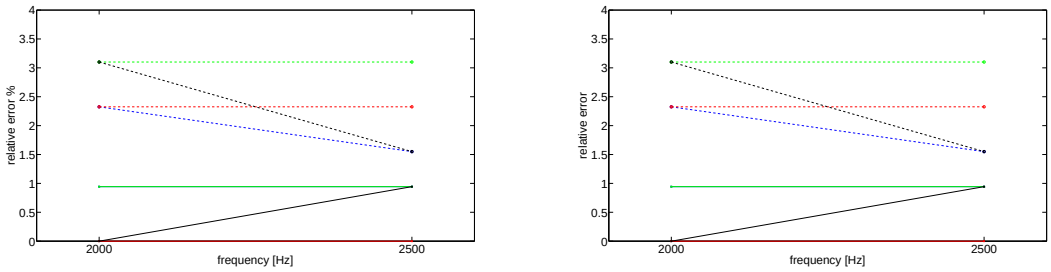

(a) Plane mode excitation

(b) Pulse excitation

Figure 10: Relative error between Z_{wr} and Z_w as a function of frequency for non uniform mean flow (– $M_0 = 0.11$ real part, – $M_0 = 0.04$ real part, – $M_0 = 0.08$ real part, – $M_0 = 0.1$ real part, - - $M_0 = 0.11$ imaginary part, - - $M_0 = 0.04$ imaginary part, - - $M_0 = 0.08$ imaginary part, - - $M_0 = 0.1$ imaginary part)

4 Conclusion

In this paper an improvement of the time domain impedance boundary condition based on recursive convolution is developed and validated. The new formulation accounts for the presence of non uniform sub stage within a time steps in the discretization of time-axis. In particular it is assumed that the time-axis is discretized using a multi-stage explicit time-integration scheme, with a constant time step Δt, subdivided in a number of stages whose length is not necessarily equal The formulation is implemented in an in house Runge-Kutta Discontinous Galerkin solver for LEE. The integration scheme used is an 8-stage Runge-Kutta fourth order scheme optimized for maximum stable time step. The case of a $2D$ rectangular duct fully lined on the bottom wall is analyzed to understand if the new implemented time domain impedance boundary condition works for cases in which a non-uniform mean flow with a finite boundary layer over the lined wall is present. The model is first validated without flow and for a uniform mean flow with Mach number $M = 0.1$. The results obtained for different lengths of the duct and for different excitation frequencies show very good agreement with analytic reference solutions. However, as soon as $\lambda/L > 0.4$, the results are affected by some oscillations over the expected main behavior. These oscillations are most probably due to some resonances caused by the interaction of the impedance boundary layer and the non reflecting boundary layer downstream. At a second stage the case of a non uniform mean flow with a boundary layer thickness of $1/10$ of the duct's height is studied. Comparing the value of the wall impedance Z_{wr} with the one imposed as boundary condition, the relative error appears to be always less than 3.5%.
Future work involves the validation of the recursive convolution formulation with a broadband frequency domain model for the impedance. Moreover an investigation at higher Mach numbers and for thinner boundary layers will be carried out.

Acknowledgements

The authors acknowledge the support of the EU Seventh Framework Programme (FP7) under the Marie Curie ITN FLOWAIRS project (GA 289352) and the Level 1 Collaborative Project IDEALVENT (GA 314066). The research of Hervé Denayer is funded by a fellowship of the Agency for Innovation by Science and Technology in Flanders (IWT). The Research Fund KU Leuven is also gratefully acknowledged for its support.

References

[1] Y. Reymen, M. Baelmans, W. Desmet, *Efficient implementation of Tam and Auriault's time-domain impedance boundary condition*, AIAA Journal, Vol. 46, pp. 2368-2376, Sep. 2008

[2] M. Muriel Gracia, B. Vanelderen, W. De Roeck, W. Desmet, *Accurate interfacing schemes for the coupling of CFD data with high order DG methods for aeroacoustic propagation*, *Proceedings of ISMA2014*, 15-17 September 2014, Leuven, Belgium

[3] T. Toulorge, *Efficient Runge Kutta Discontinuous Galerkin Methods Applied to Aeroacoustics*, PhD Thesis, KU Leuven, 2008.

[4] S.W. Rienstra, *Impedance models in time domain including the extended Helmoltz resonator model*, *Proceedings of the 12th AIAA/CEAS Aeroacoustics Conference*, AIAA 2006-2686, 8-10 May 2006, Cambridge, MA, USA

[5] Y. Reymen, *3D High-order Discontinuous Galerkin Methods for time-domain simulation of flow noise propagation*, PhD Thesis, KU Leuven, 2012.

[6] W. De Roeck, W. Desmet, *Indirect acoustic impedance determination in flow ducts using a two-port formulation*, *Proceedings of the 15th AIAA/CEAS Aeroacoustics Conference*, AIAA 2009-3302, 11-13 May 2009, Miami, FL, USA

[7] L. Enghardt, A. Fischer, *Determination of the impedance for lined ducts with grazing flow*, *Proceedings of the 18th AIAA/CEAS Aeroacoustics Conference*, AIAA 2012-2243, 04-06 June 2012, Colorado Springs, CO, USA

[8] D.C. Pridmore-Brown, *Sound Propagation in a Fluid Flowing through an Attenuating Duct*, Journal of Fluid Mechanics, Vol.4, pp.393-406, Aug. 1958

A Single frequency time-domain model

According to Reymen [5], the single-frequency model used in this work is based on the 3-parameters model:

$$Z(\omega) = \frac{Z_{-1}}{j\omega} + Z_0 + Z_1(j\omega) = \frac{(j\omega)^2 Z_1 + (j\omega)Z_0 + Z_{-1}}{j\omega}. \tag{24}$$

For the impedance model to be physically feasible, it has to be causal, real and passive [4]. This requires the Z_i to be positive. To apply the recursive convolution method, the impedance should be expressed as the sum of first and second order systems. To use this model (24), the admittance formulation is used.

$$A(\omega) = \frac{j\omega}{(j\omega)^2 Z_1 + (j\omega)Z_0 + Z_{-1}} = \frac{C(j\omega) + D}{(j\omega + \alpha)^2 + \beta^2} \tag{25}$$

If the poles of the denominator are complex conjugates $a(t)$ is real, and if the real part α is non negative, causality is also ensured.

$$a(t) = e^{-\alpha t}\left(C\cos\beta t + \frac{D - \alpha C}{\beta}\sin\beta t\right) H(t) \tag{26}$$

$$C = \frac{1}{Z_1} \quad D = 0 \quad \alpha = \frac{Z_0}{(2Z_1)} \quad \beta = \sqrt{\frac{Z_{-1}}{Z_1} - \alpha^2} \tag{27}$$

Equation (27) shows the relation between C, D, α, β and Z_1, Z_0, Z_{-1}, which can be related to the resistance R and the reactance X of the impedance at the design frequency $\bar{\omega}$, using following formulation.

$$Z(\bar{\omega}) = R + jX = Z_0 + j\left(Z_1\bar{\omega} - \frac{Z_{-1}}{\bar{\omega}}\right) \tag{28}$$

Using equation (28) the relation between R and Z_0 is evident. Moreover, since R is always positive, the model is , by definition, passive. The reactance can be formulated based on the other two parameters using an arbitrary weighting factor g.

$$\begin{aligned} Z_0 = R \;\; Z_1 = \frac{(1+g)|X|}{\bar{\omega}} \;\; and \;\; Z_{-1} = g|X|\bar{\omega} \;\; if \;\; X > 0 \\ Z_1 = \frac{g|X|}{\bar{\omega}} \;\; and \;\; Z_{-1} = (1+g)|X|\bar{\omega} \;\; if \;\; X < 0 \end{aligned} \tag{29}$$

To ensure that β is real and Z_{-1} and Z_1 are positive, g is subject to the following condition:

$$g \geq \frac{\left(-1 + \sqrt{1 + \left(\frac{R}{X}\right)^2}\right)}{2}. \tag{30}$$

B Proof of the recursive relations for χ_k^m and $\hat{\xi}_l^m$

Computing the integral:

$$\chi_k^m = \int_{m\Delta t}^{(m+1)\Delta t} e^{-\lambda_k \tau}\, d\tau = \frac{e^{-\lambda_k m\Delta t} - e^{-\lambda_k (m+1)\Delta t}}{\lambda_k} \tag{31}$$

$$= \frac{e^{-\lambda_k m\Delta t}\left(1 - e^{-\lambda_k \Delta t}\right)}{\lambda_k} \tag{32}$$

Since Δt is constant, this means that:

$$\begin{aligned}\chi_k^{m+1} &= \frac{e^{-\lambda_k (m+1)\Delta t}\left(1 - e^{-\lambda_k \Delta t}\right)}{\lambda_k} \\ &= \frac{e^{-\lambda_k m\Delta t} e^{-\lambda_k \Delta t}\left(1 - e^{-\lambda_k \Delta t}\right)}{\lambda_k} \\ &= e^{-\lambda_k \Delta t}\, \chi_k^m \end{aligned} \tag{33}$$

Computing the integral in the definition of ξ_k^m, using integration by parts:

$$\xi_k^m = \frac{1}{\Delta t} \int_{m\Delta t}^{(m+1)\Delta t} e^{-\lambda_k \tau}\,(\tau - m\Delta t)\; d\tau \tag{34}$$

$$= \frac{1}{\Delta t}\left(\left[\frac{e^{-\lambda_k \tau}\,(\tau - m\Delta t)}{-\lambda_k}\right]_{m\Delta t}^{(m+1)\Delta t} + \frac{1}{\lambda_k} \int_{m\Delta t}^{(m+1)\Delta t} e^{-\lambda_k \tau}\, d\tau \right) \tag{35}$$

$$= \frac{1}{\lambda_k \Delta t}\left(-\Delta t\, e^{-\lambda_k (m+1)\Delta t} + \chi_k^m\right) \tag{36}$$

Hence:

$$\xi_k^{m+1} = \frac{1}{\lambda_k \Delta t}\left(-\Delta t\, e^{-\lambda_k (m+2)\Delta t} + \chi_k^{m+1}\right) \tag{37}$$

$$= \frac{e^{-\lambda_k \Delta t}}{\lambda_k \Delta t}\left(-\Delta t\, e^{-\lambda_k (m+1)\Delta t} + \chi_k^m\right) \tag{38}$$

$$= e^{-\lambda_k \Delta t} \xi_k^m \tag{39}$$

Replacing λ_k by $(\alpha_l - j\beta_l)$ proofs the relations for $\hat{\chi}_l^m$ and $\hat{\xi}_l^m$:

$$\hat{\chi}_l^{m+1} = e^{(-\alpha_l + j\beta_l)\Delta t}\, \hat{\chi}_l^m \qquad\qquad \hat{\xi}_l^{m+1} = e^{(-\alpha_l + j\beta_l)\Delta t}\, \hat{\xi}_l^m \tag{40}$$

C Proof of the recursive relations for ψ_k^n and $\hat{\psi}_l^n$

Recalling the definitions:

$$\psi_k^n = \sum_{m=0}^{n-1} \left(p^{n-m} \chi_k^m + \left(p^{n-m-1} - p^{n-m}\right) \xi_k^m\right) \tag{41}$$

$$\hat{\psi}_l^n = \sum_{m=0}^{n-1} \left(p^{n-m} \hat{\chi}_l^m + \left(p^{n-m-1} - p^{n-m}\right) \hat{\xi}_l^m\right) \tag{42}$$

Taking $m = 0$ out of the summation:

$$\psi_k^n = \left(p^n \chi_k^0 + \left(p^{n-1} - p^n\right) \xi_k^0\right) + \sum_{m=1}^{n-1} \left(p^{n-m} \chi_k^m + \left(p^{n-m-1} - p^{n-m}\right) \xi_k^m\right) \tag{43}$$

$$\hat{\psi}_l^n = \left(p^{n-m} \hat{\chi}_l^0 + \left(p^{n-1} - p^n\right) \hat{\xi}_l^0\right) + \sum_{m=1}^{n-1} \left(p^{n-m} \hat{\chi}_l^m + \left(p^{n-m-1} - p^{n-m}\right) \hat{\xi}_l^m\right) \tag{44}$$

Renumbering the summation:

$$\psi_k^n = \left(p^n \chi_k^0 + \left(p^{n-1} - p^n\right) \xi_k^0\right) + \sum_{m=0}^{m-2} \left(p^{n-1-m} \chi_k^{m+1} + \left(p^{n-1-m-1} - p^{n-1-m}\right) \xi_k^{m+1}\right) \tag{45}$$

$$\hat{\psi}_l^n = \left(p^{n-m} \hat{\chi}_l^0 + \left(p^{n-1} - p^n\right) \hat{\xi}_l^0\right) + \sum_{m=0}^{n-2} \left(p^{n-1-m} \hat{\chi}_l^{m+1} + \left(p^{n-1-m-1} - p^{n-1-m}\right) \hat{\xi}_l^{m+1}\right) \tag{46}$$

And using the relations proven in appendix B:

$$\psi_k^n = \left(p^n \chi_k^0 + \left(p^{n-1} - p^n\right) \xi_k^0\right) + e^{-\lambda_k \Delta t} \sum_{m=0}^{n-2} \left(p^{n-1-m} \chi_k^m + \left(p^{n-1-m-1} - p^{n-1-m}\right) \xi_k^m\right) \tag{47}$$

$$\hat{\psi}_l^n = \left(p^{n-m} \hat{\chi}_l^0 + \left(p^{n-1} - p^n\right) \hat{\xi}_l^0\right) + e^{(-\alpha_l + j\beta_l)\Delta t} \sum_{m=0}^{n-2} \left(p^{n-1-m} \hat{\chi}_l^m + \left(p^{n-1-m-1} - p^{n-1-m}\right) \hat{\xi}_l^m\right) \tag{48}$$

Or:

$$\psi_k^n = p^n \chi_k^0 + \left(p^{n-1} - p^n\right) \xi_k^0 + e^{-\lambda_k \Delta t} \psi_k^{n-1} \quad \hat{\psi}_l^n = p^n \hat{\chi}_l^0 + \left(p^{n-1} - p^n\right) \hat{\xi}_l^0 + e^{(-\alpha_l + j\beta_l)\Delta t} \hat{\psi}_l^{n-1} \tag{49}$$